Impact of Cloud-Nucleating Aerosols in Cloud-Resolving Model Simulations of Warm-Rain Precipitation in the East China Sea

STEPHEN M. SALEEBY, WESLEY BERG, SUSAN VAN DEN HEEVER, AND TRISTAN L'ECUYER

Colorado State University, Fort Collins, Colorado

(Manuscript received 8 April 2010, in final form 26 July 2010)

ABSTRACT

Cloud-nucleating aerosols emitted from mainland China have the potential to influence cloud and precipitation systems that propagate through the region of the East China Sea. Both simulations from the Spectral Radiation-Transport Model for Aerosol Species (SPRINTARS) and observations from the Moderate Resolution Imaging Spectroradiometer (MODIS) reveal plumes of pollution that are transported into the East China Sea via frontal passage or other offshore flow. Under such conditions, satellite-derived precipitation estimates from the Tropical Rainfall Measuring Mission (TRMM) Microwave Imager (TMI) and Precipitation Radar (PR) frequently produce discrepancies in rainfall estimates that are hypothesized to be a result of aerosol modification of cloud and raindrop size distributions. Cloud-resolving model simulations were used to explore the impact of aerosol loading on three identified frontal-passage events in which the TMI and PR precipitation estimates displayed large discrepancies. Each of these events was characterized by convective and stratiform elements in association with a frontal passage. Area-averaged time series for each event reveal similar monotonic cloud and rain microphysical responses to aerosol loading. The ratio in the vertical distribution of cloud water to rainwater increased. Cloud droplet concentration increased and the mean diameters decreased, thereby reducing droplet autoconversion and collision–coalescence growth. As a result, raindrop concentration decreased, while the drop mean diameter increased; furthermore, average rainwater path magnitude and area fraction both decreased. The average precipitation rate fields reveal a complex modification of the timing and spatial coverage of rainfall. This suggests that the warm-rain microphysical response to aerosols, in addition to the precipitation life cycle, microphysical feedbacks, and evaporative effects, play an important role in determining surface rainfall.

1. Introduction

With the expanse of global industrialization, there has been an increase in observed pollution and aerosol concentrations compared to preindustrial periods (Takemura et al. 2005). Recent satellite observations of aerosol optical depth (AOD), retrieved over ocean areas, reveal increases along continental coastlines and downwind maritime locations associated with desert regions and areas with high levels of fossil fuel burning (Berg et al. 2006). Models that utilize global chemical emissions databases for producing global aerosol concentrations display particularly dense aerosol coverage over the most industrialized areas of the globe, with the area of eastern China and the East China Sea exhibiting consistently high levels of AOD (Takemura et al. 2005; Berg et al. 2008). Many of these aerosols are hygroscopic and behave as cloud condensation nuclei (CCN), thereby altering cloud properties relative to clouds developing in a clean environment.

Numerous observational and modeling studies have shown that the a change in CCN number concentration leads to a modification of the cloud droplet size distribution (DSD) and subsequent precipitation formation (e.g., Rosenfeld 1999; Saleeby and Cotton 2004; Lynn et al. 2005; Pinsky et al. 2008; Cheng et al. 2009; Lee et al. 2009). (Hereinafter, the notation for CCN number concentration will be given as [CCN]). These results are generally consistent with the aerosol indirect effects proposed by Twomey (1977) and Albrecht (1989). For a given increase in [CCN], the degree of modification to the cloud DSD is a function of a cloud's macrophysical properties, such as liquid water content (LWC), its internal dynamics, and its environment. Feingold (2003), for example, demonstrated that at high LWC, more aerosols

Corresponding author address: Stephen M. Saleeby, Atmospheric Science Department, Colorado State University, Fort Collins, CO 80523.
E-mail: smsaleeb@atmos.colostate.edu

DOI: 10.1175/2010JAS3528.1

are needed to reduce the mean droplet size to the point where collision–coalescence growth and precipitation formation are suppressed.

Simulations of precipitating marine cumuli have revealed a complicated scenario in which dynamic feedbacks to the cloud system occur following initial formation in the presence of enhanced aerosol loading (Jiang et al. 2002, 2006; Xue and Feingold 2006; Cheng et al. 2009). In these types of clouds, a high [CCN] tended to reduce droplet size, narrow the droplet spectrum, limit droplet autoconversion, and suppress precipitation. There was an initial increase in cloud depth, cloud-top height, and liquid water path (LWP) due to greater buoyancy production from increased latent heat release via droplet nucleation and condensation growth. However, following initial formation and growth, the LWP was reduced along with cloud fraction and lifetime resulting from more efficient cloud-top and midlevel lateral entrainment and evaporation, suggesting that aerosol impacts vary dramatically over the life cycle of the cloud system.

In the shallower environment of subtropical marine stratocumulus clouds, Lee et al. (2009) and Wood (2007) found a similar dynamical growth response to aerosol loading in which polluted clouds initially grew deeper via enhanced latent heat production in spite of cloud-top entrainment. However, once these clouds begin precipitating the degree of subcloud evaporation and the cloud-base height were found to modulate the magnitude of subcloud-layer stability and turbulence. The environmental temperature and moisture profiles in which these clouds form play a large role in determining whether aerosol loading will ultimately result in thinner or thicker clouds and enhanced or suppressed precipitation.

From a remote sensing perspective, Rosenfeld (1999) and Berg et al. (2006, 2008) examined satellite estimates of precipitation rate from the Tropical Rainfall Measuring Mission (TRMM) Microwave Imager (TMI) and Precipitation Radar (PR) over oceanic regions impacted by high levels of pollution aerosols. While both the passive (TMI) and active (PR) sensors on board TRMM were designed for retrieving estimates of rainfall, they rely on different physical principals to obtain those estimates. The active PR sensor estimates rainfall based on the size and number of precipitation hydrometeors and has a minimal detectable signal of ~17 dBZ, making it insensitive to light rain (less than approximately 0.5 mm h^{-1}). The TMI passive sensor estimates rainfall based on attenuation through a cloud, which makes it sensitive to condensate path and changes in precipitation efficiency. A comparison between clouds in polluted and unpolluted areas by Rosenfeld (1999) revealed reduced precipitation-sized particles from the PR and larger cloud water content from the TMI in the polluted clouds, thus implying that these global satellite datasets may be capable of discerning an aerosol signature in precipitating clouds.

This finding is reinforced by the studies of Berg et al. (2006, 2008), who showed that whereas global satellite estimates of precipitation rate from the TMI and PR sensors differ by less than 0.5 mm day^{-1} in many regions, the region from southeastern China extending across the East China Sea to Japan shows a difference of over 2.0 mm day^{-1} averaged over the winter and early spring. The location of largest precipitation differences corresponds to that of the observed and modeled high concentration of aerosols near eastern China. This result would tend to support the assertion that aerosols induce substantial changes in the microphysical properties of clouds over this region, and it suggests that this region may be an excellent target for cloud-resolving-model (CRM) simulations to investigate this further.

Toward these ends, Berg et al. (2008) used idealized CRM simulations to generate a time-evolving, multicloud-type system within an environment representative of the East China Sea. Simulations with varying amounts of aerosol loading revealed a transition from convective to stratiform precipitation with reduced LWP during the convective phase and increased LWP during the stratiform period in more polluted conditions resulting from an increase in the cloud water to rainwater ratio. With high [CCN] these idealized simulations exhibited an initial delay in rain formation and reduced accumulation followed by a reversal during the stratiform period toward higher rain accumulation.

The goal of this study is to build on these idealized simulations and use high-resolution numerical model simulations of real events to investigate the impacts of [CCN] on marine cumuli and stratocumuli cloud systems in association with frontal passages near the East China Sea where pollution levels are high and where the satellite observations suggest that aerosol effects may be quite frequent and substantial. The studies mentioned above reveal varying responses to [CCN] between convective and stratiform maritime cloud systems. They also reveal that the life cycle and variability in dynamic feedbacks can alter the aerosol response during various cloud phases. Because of the potential variability in aerosol response among cloud types and cloud life cycle it is presumptive to apply results of idealized studies in an attempt to understand the role of aerosols in modification of cloud microphysical properties and precipitation in the polluted region of the East China Sea. We seek, therefore, to determine how changes in [CCN] over the East China Sea may influence vertical cloud structure, cloud and raindrop spectra, cloud and rainwater paths, and rainfall rate as well as to determine if

there are aerosol effects that exhibit consistent and predictable responses to changes in [CCN] for various model-simulated events.

2. Model and experiment configuration

To investigate the impacts of aerosol loading on these large-scale systems near the East China Sea, nonidealized CRM simulations were performed for a number of events in which the Spectral Radiation-Transport Model for Aerosol Species (SPRINTARS) model and satellite retrievals indicated high AOD and the TMI and PR rainfall retrievals exhibited substantial differences in the detection and intensity of rainfall. The initial selected cases were chosen from among several years of data that compare the TMI and PR estimates of precipitation over the East China Sea. Berg et al. (2008) note the consistent and prolonged differences that exist over this region during winter and spring months when baroclinic systems are quite common.

From among the possible cases, three events were chosen for further sensitivity simulations. The chosen events best met the following criteria: 1) there were large differences between TMI and PR retrievals, 2) the SPRINTARS data indicated a plume of pollution over the region of interest, 3) they produced the most realistic simulated cloud systems compared to satellite observations of cloud cover, and 4) and the amount of ice in the interest region was relatively small. Because of the highly variable nonspherical nature of ice particles and the potential for them to become water coated near the freezing level, resulting in brightband precipitation, the satellite retrievals tend to exhibit substantial biases in brightness temperature, LWP, and estimates of precipitation intensity (Berg et al. 2006, 2008). As such, the precipitation events chosen for sensitivity simulations in this study are primarily warm rainfall episodes with cloud tops typically below the freezing level (see Fig. 1, row 3).

The identified events occurred on 22–23 January 1998, 2–3 February 2004, and 2–3 April 2007. The April 2007 case corresponds to the idealized simulation discussed in Berg et al. (2008) and was selected for comparison to those results. Figure 1 (rows 4 and 5) displays the TMI and PR rain rates for a satellite overpass during each event. In each case the TMI reports a greater precipitation rate than the PR with the exception of areas of more intense convection on the northern part of the domain in the 2–3 April 2007 case.

Each chosen event involved the passage of a midlevel trough, as seen in the 500-hPa geopotential height field in Fig. 1 (row 1), with winds from the west or southwest in the Regional Atmospheric Modeling System (RAMS) fine-grid domain. The centers of low pressure were over 1000 km north of the area of interest near Taiwan in 1998 and 2004 and several hundred kilometers north of the domain in 2007 southeast of Japan. As such, the deepest cloud system and heaviest precipitation was focused north of Japan. The trough passages were accompanied by convective frontal lines with leading and/or trailing stratiform regions. The postfrontal stratiform regions were widespread, persisted over 24 h, and typically had cloud-top temperatures warmer than 260 K in both the satellite observations and model simulations.

The amount of liquid versus ice in these simulations was determined from calculations of the ratio of the horizontally averaged LWP to total condensate path (TCP). From the model analyses, the LWP is the vertical column integrated liquid condensate mass expressed in terms of liquid water equivalent depth (mm). LWP is the sum of the cloud water path (CWP) and rainwater path (RWP), and the TCP is the sum of the LWP and ice water path (IWP). The time series of LWP/TCP were examined for all simulations from each case study. For the 1998 event, the liquid water percentage remained at 95% or higher for the duration of the event. In the 2004 case, the percentage of liquid water never dropped below 85%, and was above 95% most of the time. The 2007 event occurred farther north but had a liquid water percentage of 75%–95% for the duration, with the majority of the time containing greater than 90% liquid condensate. While the 2007 event does contain more ice than the other two events, it was included in this study since it was examined in detail by Berg et al. (2008) and did exhibit signs of possible aerosol impacts within the warm rain areas of the domain.

The Regional Atmospheric Modeling System developed at Colorado State University was used for this study (Cotton et al. 2003). The Spectral Radiation-Transport Model for Aerosol Species (Takemura et al. 2000, 2005) was used to obtain baseline [CCN] vertical profiles over the simulated regions. Figure 1 (row 1) displays the 500-hPa geopotential height field and winds for each event along with the overlaid RAMS grid configuration. The grid arrangement consisted of three interactive grids with two-way nesting. The precipitation systems in the three simulated events occurred in different locations so that the grid locations are different but the grid sizes are the same. The outer grid (grid 1) consisted of 100×84 horizontal grid points in the x and y directions with 25-km grid spacing. Maximum nesting ratios should typically not exceed 5:1, so grids 2 and 3 have horizontal spacing of 5 km and 1.25 km (102×132 grid points and 362×462 grid points), respectively. The vertical grid spacing for all domains was 75 m at the surface and was gradually stretched to 850 m above 8 km.

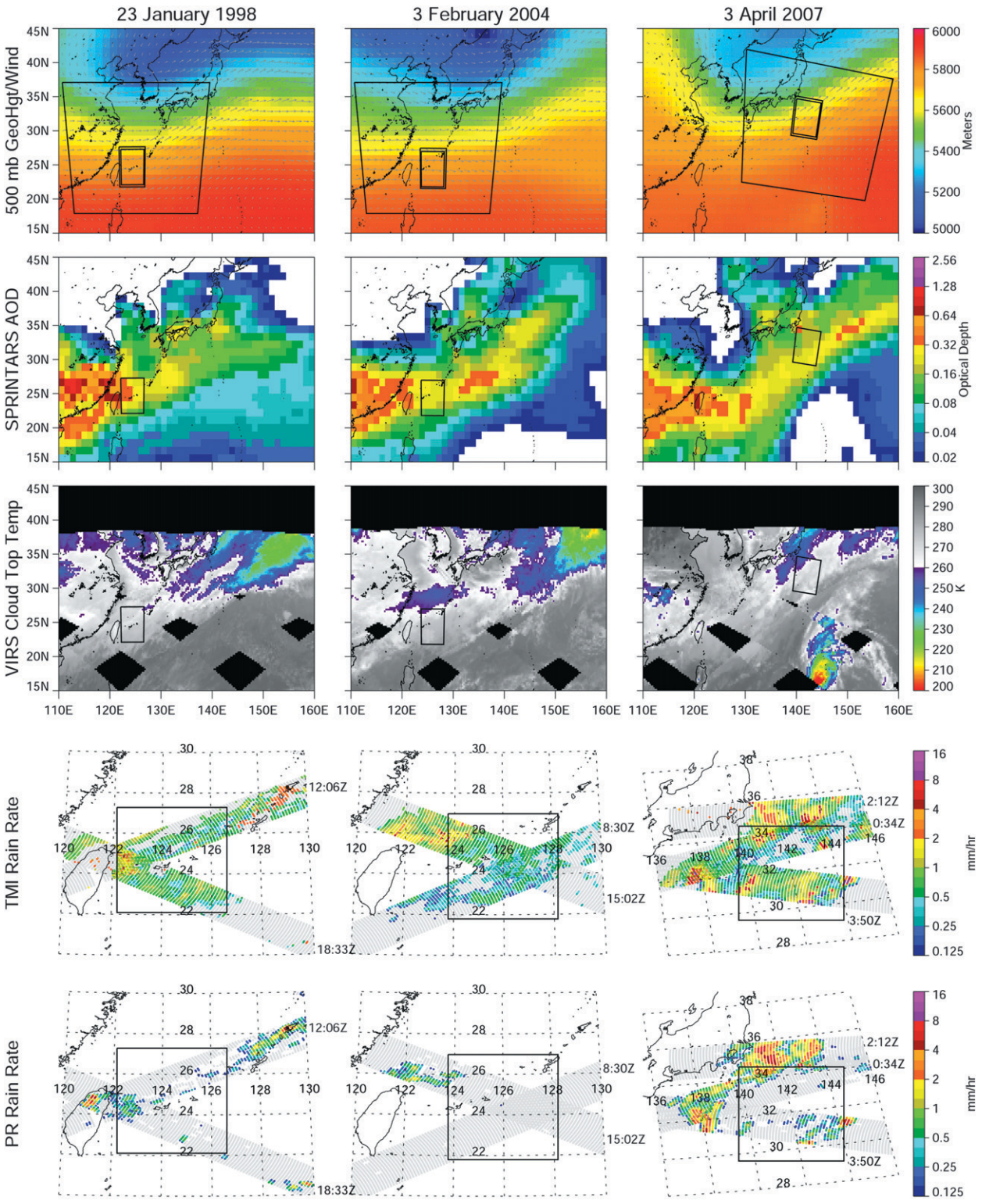

FIG. 1. (row 1) Geopotential height contours (m) and wind (m s^{-1}) and placement of model grids for the three events of 23 Jan 1998, 3 Feb 2004, and 3 Apr 2007, (row 2) SPRINTARS model AOD, (row 3) VIRS cloud-top temperature (K), (row 4) TMI rainfall rate (mm h^{-1}), and (row 5) PR rainfall rate (mm h^{-1}).

On 32-bit computing systems, the system memory is a limiting factor to grid size and resolution; as such, we chose to maximize the size of grid 3 by keeping grid 2 only slightly larger than grid 3. This allows more memory (grid points) to be allocated to the highest-resolution grid. Future operation on 64-bit computer systems will reduce the need to impose domain size constraints. The model domains are positioned on a polar stereographic grid with pole tangent point located at 28°N, 125°E. The 1998 and 2004 events occur close to this tangent point so that little or no skewness appears in domain plots in Fig. 1; however, the 2007 event occurred east of Japan away from the model pole point, thereby resulting in some apparent skewness in the plotting relative to the other cases. This visual difference, however, does not influence the model integrity or simulation results.

The European Centre for Medium-Range Weather Forecasts (ECMWF) 1.5° reanalysis data were used for model initialization and nudging of the lateral boundaries of grid 1. The radiative boundary condition of Klemp and Wilhelmson (1978) was also applied to the lateral boundaries of grid 1. For all grids, RAMS used the hydrometeor-sensitive radiation scheme of Harrington (1997), the Land Ecosystem–Atmosphere Feedback-2 surface flux model (Walko et al. 2000), the horizontal turbulent diffusion of Smagorinsky (1963), and the vertical turbulent kinetic energy level-2.5 closure of Mellor and Yamada (1974). The Kain and Fritsch (1993) cumulus parameterization was applied to grid 1, while convection was resolved explicitly on grids 2 and 3.

Simulations used a two-moment bulk microphysics module that prognoses a mixing ratio and number concentration of cloud droplets, rain, pristine ice, snow, aggregates, graupel, and hail (Walko et al. 1995; Meyers et al. 1997). Hydrometeor spectra are represented by gamma distributions with defined shape parameters. The cloud droplet distribution uses a gamma function shape parameter $\nu = 4$, and all other hydrometeor categories use $\nu = 2$. Larger values of ν dictate a more narrow distribution.

Cloud droplet number concentration is predicted from explicit activation of CCN (Saleeby and Cotton 2004). The vertical profiles of [CCN] from SPRINTARS are initialized and nudged three-dimensionally on all grids at frequent intervals by interpolation between time-varying fields of CCN. The representative SPRINTARS fields of AOD are shown in Fig. 1 (row 2) relative to the model fine-grid domain. Each control simulation is impacted by locally high concentrations of aerosols. The cloud nucleation model activates a percentage of available CCN based on ambient vertical velocity, temperature, [CCN], and CCN median radius according to the method of Saleeby and Cotton (2004). The relationship between vertical velocity and supersaturation with respect to liquid was established using the Lagrangian parcel model of Heymsfield and Sabin (1989).

The collision–coalescence growth process of cloud droplets and rain is simulated using a bin-emulating approach by first decomposing the liquid water distribution into 36 size bins. The method-of-moments technique (Tzivion et al. 1987) is then used to solve the stochastic collection equation for probabilistic interaction of all size bins while using a realistic collection kernel based on collection efficiencies from Long (1974). The gamma function of cloud and rainwater is then restored based on the binned redistribution of liquid water. Short of running a full bin microphysics model, this approach realistically simulates the autoconversion of cloud water to rainwater as well as accretion of cloud droplets by raindrops during sedimentation. The sedimentation process also uses a similar binned approach and size-related fall speeds so that larger hydrometeors within a distribution will fall faster than smaller ones. This is far more precise than applying a single mass-weighted fall speed to an entire DSD.

For each simulated event a set of four simulations were performed with varying degrees of aerosol loading relative to the use of SPRINTARS [CCN] in the control run. Simulations were run using one-fourth of the control fields of [CCN], one-half of the control, the control run, and 2 times the control; these simulations are hereby referred to as QUAR, HALF, CTRL, and DBLE, respectively. This notation is used in subsequent figures to identify each simulation with different [CCN]. Each simulation was frequently nudged domain wide via linear time interpolation in 3D so as to force the model [CCN] to the relative SPRINTARS values. For aerosol activation and cloud droplet nucleation, the percentage of aerosols to activate and form droplets is determined from the parcel model lookup tables. Once droplets form in a given time step, additional nucleation only occurs if supersaturation supports additional droplets. Since [CCN] is nudged to the SPRINTARS 3D field and CCN are not explicitly removed upon activation, the number concentration of droplets is limited such that it can never exceed the grid cell concentration of CCN.

3. Simulation results

a. Precipitation rate

The average precipitation rate for each event and sensitivity simulation is displayed in Fig. 2. The analysis in this figure and all that follow represent model results on the highest-resolution grid with 1.25-km grid spacing. While [CCN] is varied substantially from QUAR to DBLE, the overall depiction of precipitation is similar

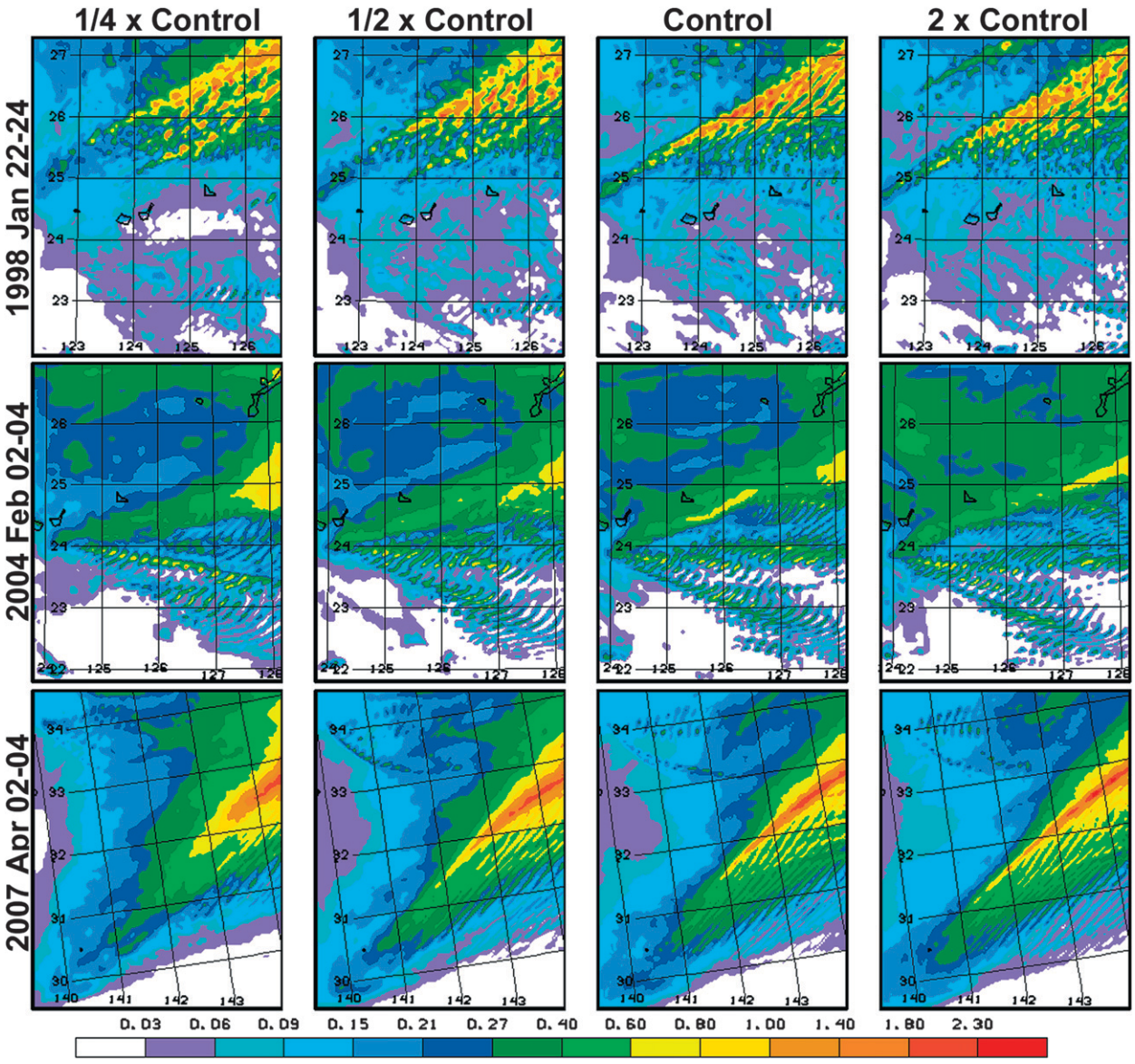

FIG. 2. Averaged precipitation rate (mm h^{-1}) for (from left to right) the ¼ × Control, ½ × Control, Control, and 2 × Control simulations (labeled on top) for the simulated events from (top) 22–24 Jan 1998, (middle) 2–4 Feb 2004, and (bottom) 2–4 Apr 2007. Here Control represents use of the SPRINTARS-derived CCN concentration; for example, 2 × Control uses a CCN concentration field that is twice the Control concentration.

among sensitivity tests. It is evident from comparison among sensitivity experiments that one cannot make a blanket statement of precipitation suppression or enhancement as [CCN] is increased. Instead, we see areas of both suppression and enhancement across the domain in each event. In such complex frontal cases in which there is continual evolution of the system driven by the large-scale dynamics, the change in [CCN] will make an initial modification to the cloud field. This modification will then perpetuate in time and continually alter the system in a very nonlinear fashion that is less predictable than a simulation of short-term cloud development from initiation to maturity to dissipation.

Each event exhibits periods of convection indicated by the banded structures of greater precipitation rate in each panel of Fig. 2. The increase in [CCN] from QUAR to DBLE appears to lead to narrower bands of heavy precipitation. This is particularly noticeable in the 1998 and 2007 events, which have overall more intense precipitation. These more narrow aligned bands tend to be more intense (>1.00 mm h^{-1}) at their maxima but exhibit reduced areas of moderate averaged precipitation

rate (0.21–0.60 mm h^{-1}) surrounding the convective precipitation line. It is plausible that higher [CCN] leads to greater cloud production, greater latent heat release, and stronger local updrafts that intensify but narrow the line of convection. In effect, increasing [CCN] may be changing a broad area of moderate lift into a focused narrow area of strong lift by modifying the underlying cloud and rain development processes, which in turn will alter precipitation and surface cold pools that can feed back into subsequent convective growth.

b. *Cloud droplet and raindrop microphysical characteristics*

For a given supersaturation, an increase in [CCN] should initially modify cloud development by leading to nucleation of a greater number of smaller cloud drops. Over time this would affect cloud lifetime, cloud fraction, LWP, CWP, RWP, and rain formation to varying degrees over the evolution of these long-lived frontal systems. As such, we will be examining the time series of domain-averaged quantities to determine if there is some periodicity in aerosol effects in a domain-wide sense or if the underlying microphysical response to increased aerosols is consistent over time. Figure 3 displays the time series of cloud droplet number concentration (CDNC), droplet mean mass diameter, and CWP for each event and sensitivity simulation. The domain-wide averages of CDNC and mean diameter were limited to grid cells with a minimum cloud mixing ratio of 0.05 g kg^{-1}, while averages of CWP were limited to grid columns with minimum LWP of 0.01 mm, so that cloud-free cells or grid columns would not dilute the averages. At all times and for each event, there is a nearly monotonic increase in averaged droplet number for an increase in [CCN]. Likewise, there is a monotonic decrease in mean droplet diameter for an increase in [CCN] that is consistent with time. While droplets are smallest in the DBLE simulations, their mean diameters are approximately 20 μm on average. The most polluted events are still not polluted enough to reduce mean droplet sizes toward the 10-μm cutoff reported by Pruppacher and Klett (1997) as the size below which conversion of cloud water to rainwater is severely inhibited. Regardless of the presence of primarily stratiform or convective precipitation, the basic microphysical response over the domain at the cloud formation scale is consistent with traditional thinking.

For the majority of time in the three events, CWP increases with increasing [CCN] because of both the addition of greater amounts of nucleated cloud water and the reduced autoconversion of cloud droplets to rain. However, there is some variability seen in each event regarding the trend in CWP with [CCN]. The total cloud water field will be highly susceptible to changes in exterior forcing. Inconsistencies in the CWP trend over time result from nonlinear changes in the dynamics of the system, which will modify nucleation rate, autoconversion and accretion, entrainment and evaporation, and precipitation efficiency; the balance of these processes determine the net amount of suspended cloud water.

Droplet autoconversion and subsequent accretion of cloud water by falling raindrops are the primary sources of rainwater. Vapor diffusion growth also contributes to rainwater, but to a lesser degree. However, it will be shown later that evaporative effects do have a large impact on distribution of rainwater. Figure 4 displays a plot similar to Fig. 3 but for rain DSD attributes instead of cloud droplets. In the top row of panels in Fig. 4, the time series of raindrop number concentration display a monotonic decrease in number for an increase in [CCN]; this tendency is consistent for all times and for all simulated events. Likewise, the time series of the rain mean mass diameter reveals an increase in mean size of the rain DSD for an increase in [CCN]. This trend can be explained via the warm rain formation processes.

In polluted conditions, the autoconversion process will be limited, meaning that the random collisions of cloud droplets are less likely to form rain embryos because of the small droplet size and low self-collection efficiencies. Autoconversion will primarily determine the raindrop number concentration, while accretion of additional cloud water contributes more directly to growth of the initial rain embryos. In a polluted environment there are fewer raindrops forming by autoconversion, so there is 1) less competition among raindrops for accretion growth, 2) a greater population of cloud droplets to collect, and 3) a greater differential fall speed between small cloud droplets and large raindrops, which enhances collection efficiency. Thus, the polluted simulations lead to fewer but larger raindrops. The occurrence of larger raindrops in polluted conditions was also noted by Altaratz et al. (2007) and Berg et al. (2008).

The averaged RWP time series in the bottom row of Fig. 4, displays a monotonic decrease in RWP as [CCN] is increased. This trend agrees with the autoconversion/accretion model of rain formation with the assumption that other microphysical processes are neglected. Since the polluted case has fewer total raindrops available for collection, there is less total accretion of cloud water and transfer of liquid from cloud water to rainwater. Hence, RWP tends to be less in more polluted simulations.

However, in the 1998 event, this monotonic trend in RWP is less apparent during the peak period of rain formation. It will be shown that the peak in RWP during the 1998 event, at approximately 1900 UTC 22 January, corresponds to a maximum in vertical velocity. This suggests a period of vigorous nucleation and fairly rapid

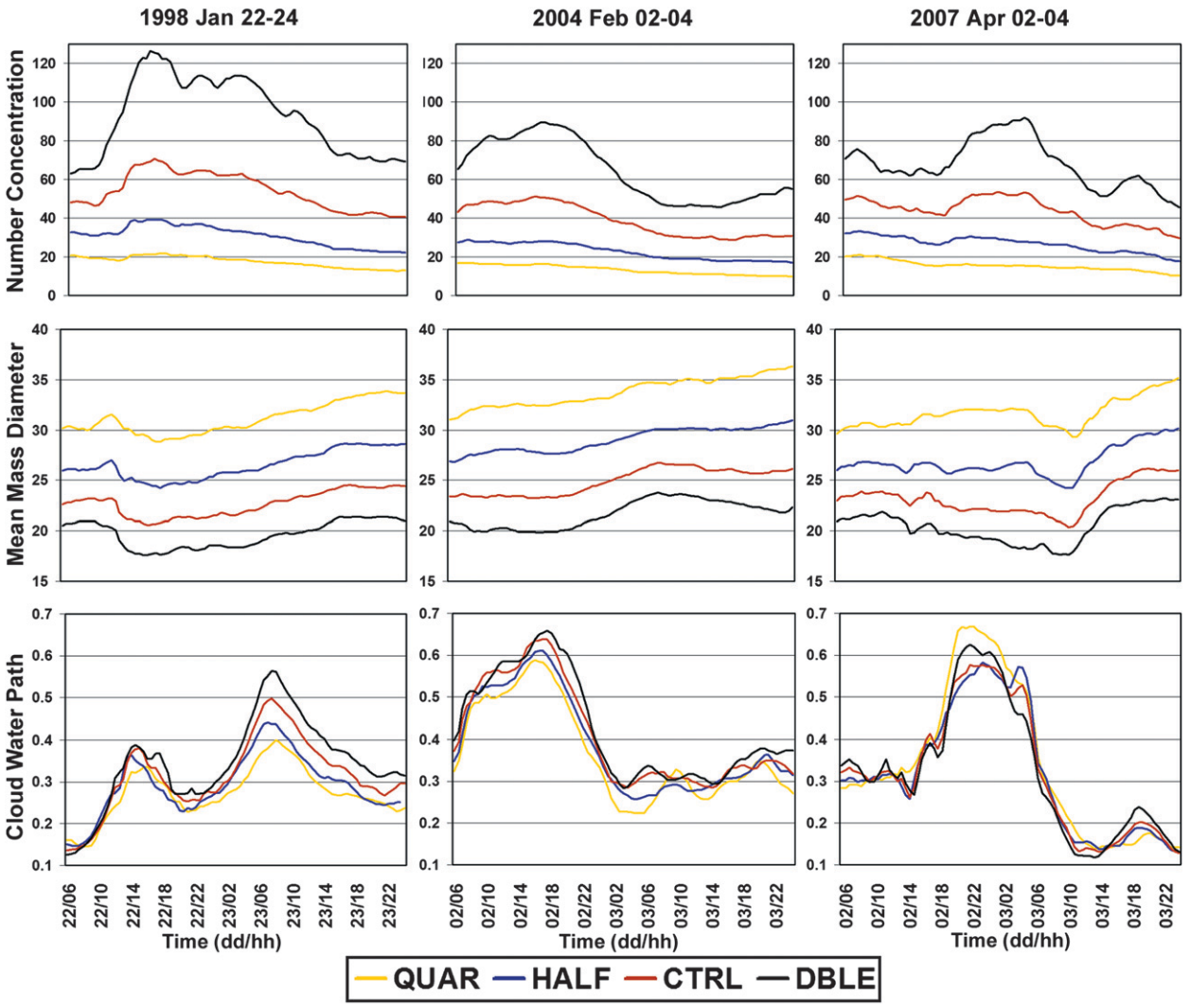

FIG. 3. Time series of (top) cloud area averaged droplet number concentration (cm^{-3}), (middle) mean mass diameter (μm), and (bottom) cloud water path (mm) for the simulated events of (left) 22–24 Jan 1998, (middle) 2–4 Feb 2004, and (right) 2–4 Apr 2007. The number concentration and mean diameter were averaged over grid cells with a minimum cloud mixing ratio of 0.05 g kg^{-1}, and cloud water path is averaged over vertically integrated horizontal grid cells with minimum LWP of 0.01 mm. The color legend displays which color line matches the appropriate simulation; QUAR = 1/4 × Control, HALF = 1/2 × Control, CTRL = Control, and DBLE = 2 × Control.

conversion of cloud water to rainwater. Since rain accretion growth in polluted conditions occurs with fewer, larger raindrops, then perhaps under vigorous environmental conditions the addition of rainwater mass occurs more efficiently with a few large drops instead of numerous smaller drops. If we examine the mean drop size of rain at this same time in the 1998 simulations, we notice an increasingly large difference between the QUAR and DBLE simulations, with maximum difference at the time of maximum RWP. The sudden rapid growth of raindrops in DBLE near 1900 UTC suggests vigorous accretion. With such rapid growth to relatively large drops, sedimentation of rain will then rapidly begin to deposit this rain field at the surface. Following this more intense convective period, the RWP trend remains clear and consistent. This effect suggests that the impact of aerosols on the total CWP and RWP is reduced during periods of stronger updrafts and deeper convection.

c. *System dynamics and rainfall*

Figure 5 displays the vertical velocity averaged over cloudy grid cells with a minimum mixing ratio of 0.05 g kg^{-1} and average surface rain rate and surface rain area percentage for grid cells with a minimum rain rate of 0.05 mm h^{-1}. For the majority of time and for each event simulated, the averaged vertical velocity is greater in the more polluted simulations. This trend is a result of greater nucleation of cloud droplets due to

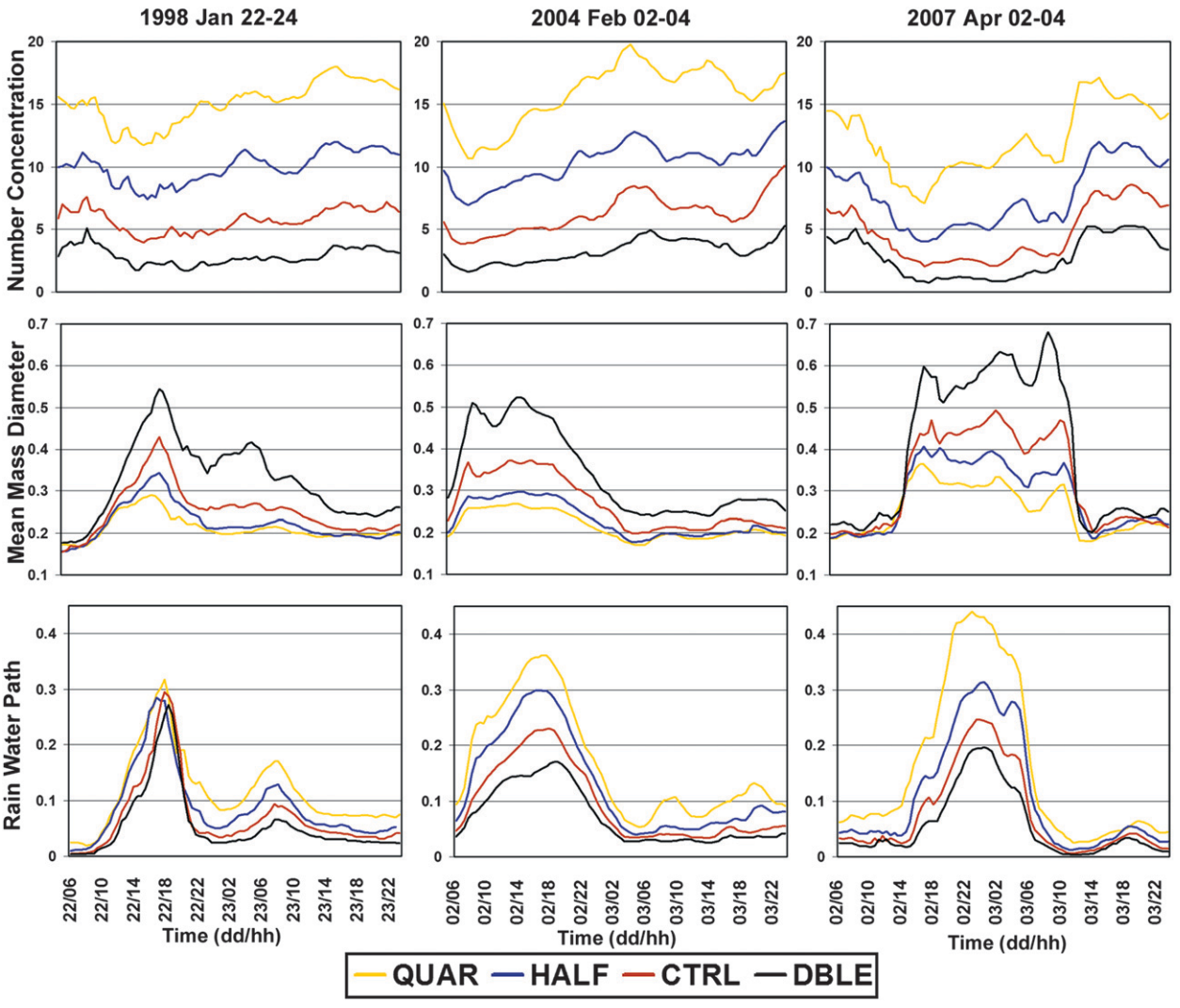

FIG. 4. As in Fig. 3, but for (top) raindrop number concentration (dm^{-3}) and (middle) mean mass diameter (mm) averaged over rainy grid cells with minimum rain mixing ratio of 0.005 g kg^{-1}, and (bottom) rainwater path (mm) averaged over vertically integrated horizontal grid cells with minimum LWP of 0.01 mm.

higher [CCN]. Enhanced latent heat release from condensation during new droplet nucleation and vapor growth leads to greater local updraft velocity. In Fig. 5, the vertical velocity scales are not the same for each event. Note that the magnitude of vertical velocity is relatively much greater in the 1998 event, especially during the convective period. While the maximum average updraft in the 2004 and 2007 events is approximately 10 cm s^{-1}, the maximum updraft in the 1998 case reaches nearly 28 cm s^{-1}. This relatively larger updraft strength may account for the less apparent CWP and RWP trends during the 1998 event on the 22 January around 1900 UTC; the stronger vertical motion may be acting as a greater control on the system compared to the impact of [CCN].

While the cloud droplet and raindrop distribution properties show substantial differences among clean and polluted simulations, the overall differences in surface rainfall rate in Fig. 5 do not reveal a great amount of variability aside from the intense period in the 1998 event discussed above. For the majority of the stratiform period with weak updraft speed, the rain rate differences are minor and there is no discernable or clear trend in rain rate change with change in [CCN]. During the more intense period of rainfall in the 1998 event the rain rate increases by over 50% for a short period of time when increasing [CCN] from QUAR to DBLE. However, the highest peak of the time series occurs for the CTRL simulation; this suggests an optimal [CCN] for peak rainfall production or perhaps this is a result of spatial

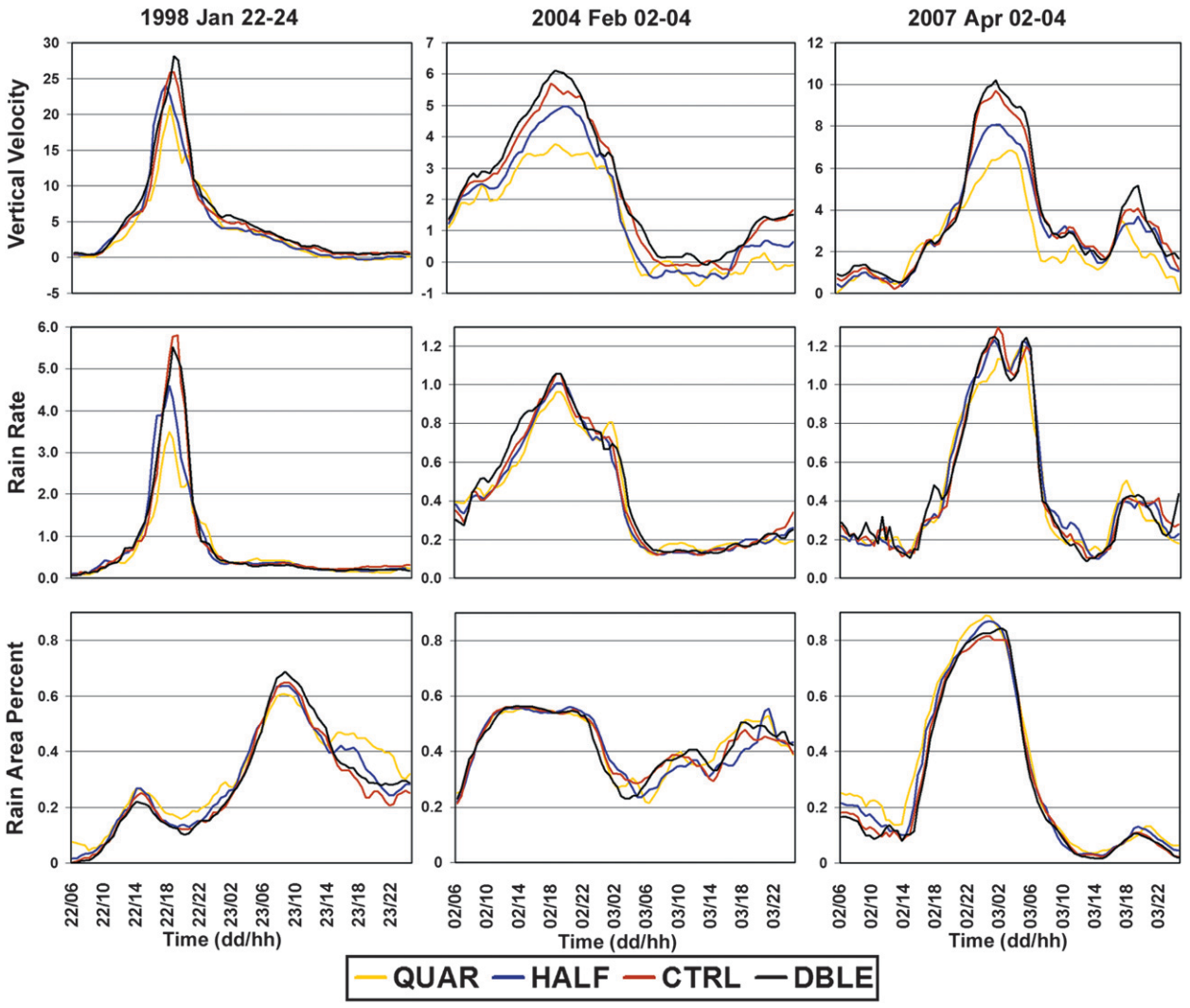

FIG. 5. As in Fig. 3, but for (top) vertical velocity (cm s^{-1}) averaged over cloudy grid cells with minimum cloud mixing ratio of 0.05 g kg^{-1}, and (middle) surface rain rate (mm h^{-1}) and (bottom) rain area coverage (%) averaged over surface grid cells with minimum surface rain rate of 0.05 mm h^{-1}.

variability in the precipitation system that impacts the resulting rain rate average. Since the rain rate trends do not differ for the majority of time among events, then perhaps rain area coverage impacts the averaging of surface rainfall rate since only rainy grid cells are factored into the plotted time series.

The bottom row of Fig. 5 displays the time series of surface rainfall area. A bulk examination of these time series does not reveal a clear trend in response to [CCN]. There is either minimal difference among time series or inconsistent variability over time as to which degree of aerosol loading produces the greatest rainfall area. If we revisit the time of 1900 UTC 22 January 22 1998, we do see greater rain area coverage for the QUAR simulation compared to DBLE. At the same time, QUAR has a relatively weaker rain rate and vertical velocity. These factors lend support toward weaker but broader frontal precipitation in clean conditions and stronger but narrower frontal precipitation in polluted conditions due to invigorated latent heat release from enhanced cloud nucleation. Again, however, the weaker precipitating periods reveal less obvious trends in rain rate and rain area coverage.

d. CWP and RWP ratio and fractional area

Aerosol loading not only modifies grid cell microphysical processes; it also impacts the partitioning of vertically integrated cloud and rainwater. The partitioning of liquid water between cloud water and rainwater, displayed in the top row of Fig. 6 as the CWP to

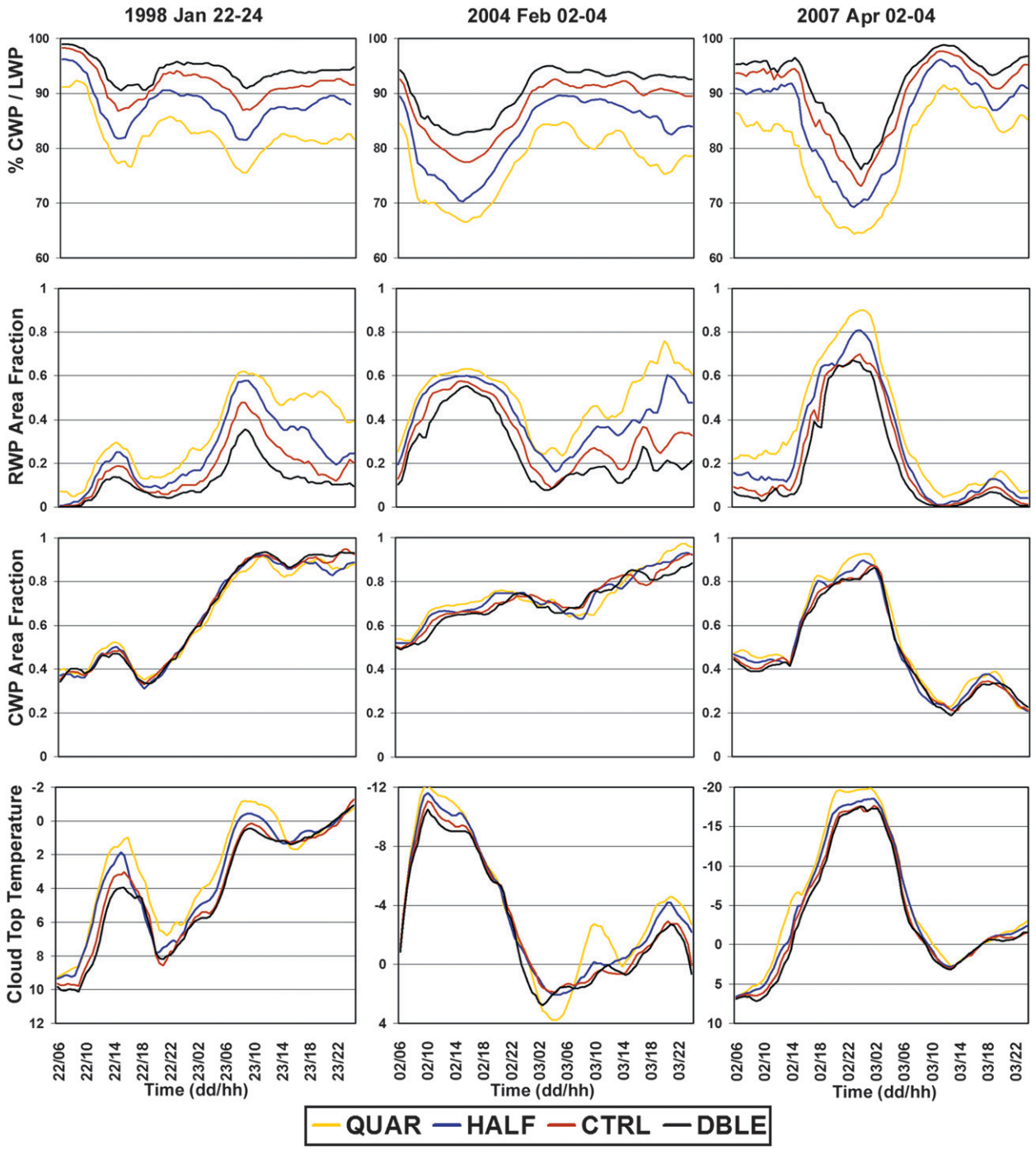

FIG. 6. As in Fig. 3, but for (first row) ratio of CWP to LWP (%), (second row) RWP area fraction, (third row) CWP area fraction, and (fourth row) cloud-top temperature (°C). Averages are taken over vertically integrated horizontal grid cells with minimum LWP of 0.01 mm.

LWP ratio percentage, is quite consistent over time and among simulated events. At all times there is a monotonic increase in CWP to LWP ratio as [CCN] is increased. This is a result of greater cloud water nucleation at high [CCN] and a reduction in cloud water removal by autoconversion and accretion due to reduced collection efficiency. This trend agrees with the trend of decreased RWP with an increase in [CCN], shown in Fig. 4. While the more polluted environment leads to fewer but larger raindrops, the total amount of rainwater produced is consistently less because of a less efficient rain formation process.

Since the averaged CWP and RWP quantities solely consider grid cells with an imposed minimum threshold, it is useful to examine the spatial coverage of cloud and rainwater. The second row of Fig. 6 shows the time series of RWP area fraction, which is essentially the fraction of the model domain with rainwater coverage in the vertical column. There is a clear trend whereby the fraction of the domain with at least a minimum RWP monotonically decreases as [CCN] is increased. A subsequent examination of the CWP fractional area, shown in the third row of Fig. 6, reveals an inconsistent and temporally varying trend in cloud cover for each simulated event. These trends suggest that dynamic lifting and supersaturation largely control cloud water formation across the domain, but the microphysical impacts of aerosols can modify the amount and spatial area of rainwater that is converted from cloud water and then precipitated out of the system.

The time series of averaged cloud-top temperature (Fig. 6, fourth row) does not reveal a definitive trend for all times relative to [CCN], but there is a tendency toward development of colder/higher cloud tops at lower [CCN]. Given the weaker averaged vertical velocity in the low [CCN] simulations (Fig. 5), it is unlikely that the higher cloud tops in the low [CCN] simulations are a result of greater cloud water production aloft. Rather, it is of greater likelihood that the high [CCN] simulations succumb to greater cloud water evaporation due to cloud-top entrainment. The smaller droplets in the polluted simulations lead to higher evaporation rates and reduced cloud tops. Given that this trend does not hold at all times, it seems that competing effects among dynamics, nucleation, collection, and evaporation all factor into the resulting maximum cloud height.

e. Rain water vertical distribution

Evaporative effects on condensed liquid water go beyond erosion of the cloud layer due to cloud-top entrainment. In subsaturated conditions, primarily near and below cloud base, the smallest particles with relatively high surface area to volume ratio succumb to evaporation at a greater rate. This effect is seen in Fig. 7 in vertical profiles of averaged rain distribution quantities. As [CCN] is increased, the vertical profiles of raindrop concentration (top row) and rain mixing ratio (bottom row) reveal decreasing magnitudes. This tends to be in agreement with the trends shown in the times series plots of rain properties in Fig. 4, in which raindrops are fewer but larger and total rainwater is reduced.

In polluted conditions the conversion of cloud water to rainwater is less efficient, but the mean raindrop sizes are larger (Fig. 7, middle row) throughout the rain portion of the averaged column. If we focus on the portion of the vertical profiles below the approximate cloud base height of 1500 m, there is a substantially greater slope in the profiles of mixing ratio and number concentration toward smaller magnitudes as [CCN] is decreased when moving from cloud base to the surface. This is a direct result of evaporation of raindrops below cloud base. Since the low [CCN] case has the highest raindrop concentration and smallest mean raindrop size, the surface area to volume ratio is relatively high and leads to large amounts of evaporation of the smallest particles. Since the smallest particles evaporate first, there is a trend toward increasing mean drop size between cloud base and the surface (Fig. 7, middle row). By the time rain reaches the surface, greater evaporation of smaller raindrops in the lower [CCN] simulations has substantially reduced the rain mixing ratio difference that exists near 1500 m AGL. If cloud base extended to the surface and the column remained nearly saturated, the surface difference in rain mixing ratio and accumulated precipitation would likely be greater and precipitation trends may appear less ambiguous.

4. Summary and conclusions

A high-resolution numerical simulation study of the aerosol effects on rainfall over the East China Sea was conducted to investigate how cloud droplet nucleating aerosols might modify the frontal and postfrontal cloud systems that frequently occur during the winter and spring months. Differences in satellite-derived precipitation rates between the passive TRMM TMI and active PR sensors frequently occur in this region during the winter and spring. The difference in satellite precipitation estimates suggests that there is spatial and temporal variability in the microphysical structure of clouds over the East China Sea. Given these frequently observed satellite discrepancies and the observed increased MODIS aerosol optical depth over this region, Berg et al. (2006, 2008) hypothesized that high concentrations of aerosols may act to modify frontal precipitation systems via modification of the cloud microphysical structure.

Three events were simulated in which the SPRINTARS estimated aerosol optical depth was high, rainfall estimates from the TMI and PR sensors exhibited substantial differences in both detection and intensity, and precipitation processes were primarily warm rain. These events were simulated using the RAMS model and were run for 48 h within a grid nest down to 1.25-km grid spacing over the area of interest for each for the following periods: 22–24 January 1998, 2–4 February 2004, and 2–4 April 2007. The estimated 3D field of CCN from the SPRINTARS aerosol transport model was used to

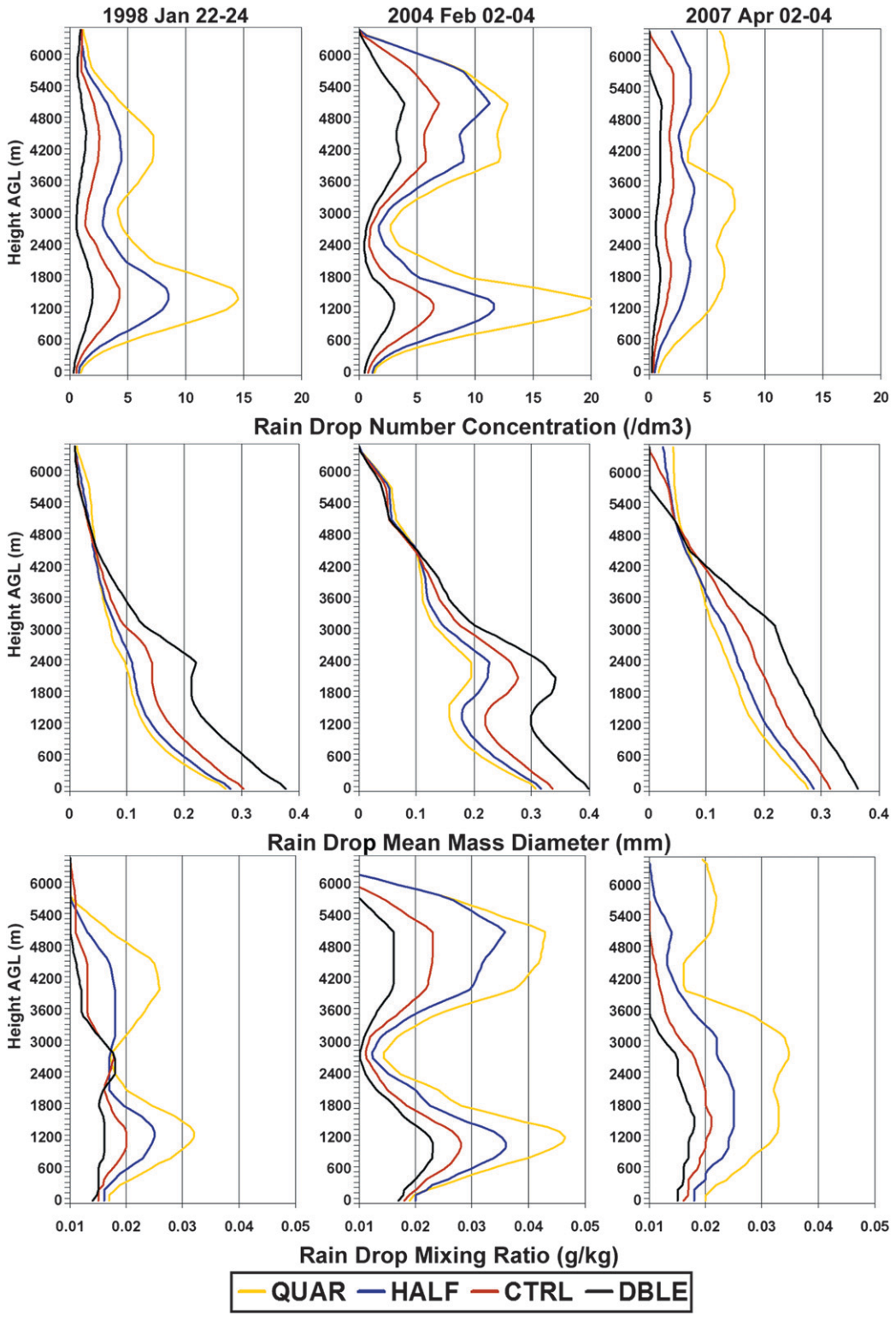

FIG. 7. Horizontally averaged vertical profiles of (top) raindrop number concentration (dm^{-3}), (middle) mean mass diameter (mm), and (bottom) mixing ratio (g kg^{-1}). Averages are taken over grid cells with minimum rain mixing ratio of 0.005 g kg^{-1}.

initialize control runs for each case. Following the control run, sensitivity simulations were run as variations of the control run. Tests included initializing and nudging of CCN number concentration at ¼ × Control, ½ × Control, and 2 × Control so as to range from clean to polluted maritime conditions.

The responses of these events to variations in CCN concentration were examined to assess whether or not aerosol loading can substantially alter the local cloud microphysical structure and resulting precipitation. The microphysical characteristics of these simulations were primarily examined as time series of cloud-area-averaged or rain-area-averaged quantities so as to investigate the evolution of the system as a whole and to determine if the response of the bulk microphysical properties remained consistent over time.

Increasing CCN concentration led to a monotonic increase in cloud droplet number concentration, decrease in cloud droplet diameter, and increase in the ratio of cloud water path to rainwater path. These trends were consistent for the full duration of each simulated event, and they agree with the standard theory of the response of the cloud droplet size distribution to increases in aerosol. The cloud water path response primarily exhibits an increase at higher CCN concentration, although there was some time variability that can be attributed to competing effects among dynamics, nucleation, and droplet removal by rain formation. The CCN impact on the raindrop size distribution follows directly from the modification of the cloud field. For an increase in CCN concentration, raindrop number concentration decreases, mean drop diameter increases, rainwater path decreases, and rainwater area fraction decreases.

The decrease in raindrop number is a result of the modification of the cloud droplet autoconversion and accretion processes. A cloud with a high number concentration of smaller droplets will have a lower probability of formation of raindrops since the autoconversion efficiency is much lower for small droplets. This leads to formation of fewer rain embryos in polluted conditions. However, once these few rain embryos form, they can continue to grow by accretion within a highly populated field of cloud droplets. This results in fewer but larger raindrops in the polluted simulations.

Vertical profiles of horizontally averaged raindrop size distribution properties point toward greater subcloud-layer evaporation in the clean simulations due to efficient evaporation of numerous small raindrops. At cloud base, the rain mixing ratio is much higher in the cleanest simulation compared to the most polluted simulation. Near the surface, the difference in rain mixing ratio is small because of greater evaporation in the cleanest simulation in this subsaturated layer. This effect helps explain the predominantly indistinguishable differences in average surface rain rate, as CCN concentration is varied, for the majority of time in each simulated event.

The aerosol effects on the modeled cloud and rain size distributions in this study agree with the idealized cloud-resolving-model simulations of Berg et al. (2008) following the initial cloud formation stage. Both studies reveal that the majority of simulation time is composed of stratiform precipitation with a tendency toward a greater amount of cloud water, reduced amount of rainwater, and higher ratio of suspended cloud water to rainwater as the number concentration of CCN is increased. These studies, however, differ with respect to precipitation response to aerosols; the idealized simulations result in an increase in rain rate with CCN concentration during the latter stratiform period whereas the real event simulations result in small and inconsistent precipitation variability. Given the similarities in the microphysical responses to nucleating aerosols between these idealized and real case studies, the differences in precipitation response between studies are likely a result of very different environmental conditions that exist between these two types of simulations. These precipitation differences among simulation types point toward a very complex chain of events that goes beyond impacts of aerosol on the cloud microphysics.

Because of the complex interaction of various aerosol types that include CCN, giant CCN, and ice nuclei, only CCN effects were investigated in this study. However, in warm rain precipitation systems, giant CCN can have a profound impact on precipitation formation (Hindman et al. 1977; Mather 1991; Feingold et al. 1999; Laird et al. 2000; Rudich et al. 2002; Saleeby and Cotton 2004; van den Heever et al. 2006). The addition of even a small concentration of giant CCN has been shown to counteract the effects of CCN. The conceptual impact of giant CCN is the enhancement of precipitation under polluted conditions by broadening the initial droplet spectrum and invigorating the collision–coalescence growth process. These effects on marine cloud systems are being investigated in an upcoming study.

Acknowledgments. The authors thank Toshihiko Takemura at Kyushu University for providing the SPRINTARS data. ERA-Interim data used in this study have been provided by ECMWF and have been obtained from the ECMWF data sever. This research was supported by the Office of Science (BER), the U.S. Department of Energy, Grant DE-FG02-08ER64572, and the National Aeronautics and Space Administration, Grant NNX07AD81G.

REFERENCES

Albrecht, B., 1989: Aerosols, cloud microphysics, and fractional cloudiness. *Science,* **245,** 1227–1230.

Altaratz, O., I. Koren, T. Reisin, A. Kostinski, G. Feingold, Z. Levin, and Y. Yin, 2007: Aerosols' influence on the interplay between condensation, evaporation, and rain in warm cumulus cloud. *Atmos. Chem. Phys. Discuss.,* **7,** 12 687–12 714.

Berg, W., T. L'Ecuyer, and C. Kummerow, 2006: Rainfall climate regimes: The relationship of regional TRMM rainfall biases to the environment. *J. Appl. Meteor. Climatol.,* **45,** 434–454.

——, ——, and S. van den Heever, 2008: Evidence for the impact of aerosols on the onset and microphysical properties of rainfall from a combination of satellite observations and cloud-resolving model simulations. *J. Geophys. Res.,* **113,** D14S23, doi:10.1029/2007JD009649.

Cheng, W. Y. Y., G. G. Carrió, W. R. Cotton, and S. M. Saleeby, 2009: Influence of cloud condensation and giant cloud condensation nuclei on the development of precipitating trade wind cumuli in a large eddy simulation. *J. Geophys. Res.,* **114,** D08201, doi:10.1029/2008JD011011.

Cotton, W. R., and Coauthors, 2003: RAMS 2001: Current status and future directions. *Meteor. Atmos. Phys.,* **82,** 5–29.

Feingold, G., 2003: Modeling of the first indirect effect: Analysis of measurement requirements. *Geophys. Res. Lett.,* **30,** 1997, doi:10.1029/2003GL017967.

——, W. R. Cotton, S. Kreidenweis, and J. Davis, 1999: The impact of giant cloud condensation nuclei on drizzle formation in stratocumulus: Implications for cloud radiative properties. *J. Atmos. Sci.,* **56,** 4100–4117.

Harrington, J. Y., 1997: The effects of radiative and microphysical processes on simulated warm and transition season Arctic stratus. Ph.D. dissertation, Dept. of Atmospheric Science, Colorado State University, 289 pp.

Heymsfield, A. J., and R. M. Sabin, 1989: Cirrus crystal nucleation by homogeneous freezing of solution droplets. *J. Atmos. Sci.,* **46,** 2252–2264.

Hindman, E. E., P. V. Hobbs, and L. F. Radke, 1977: Cloud condensation nuclei from a paper mill. Part I: Measured effects on clouds. *J. Appl. Meteor.,* **16,** 745–752.

Jiang, H., G. Feingold, and W. R. Cotton, 2002: Simulations of aerosol–cloud–dynamical feedbacks resulting from entrainment of aerosol into the marine boundary layer during the Atlantic Stratocumulus Transition Experiment. *J. Geophys. Res.,* **107,** 4813, doi:10.1029/2001JD001502.

——, H. Xue, A. Teller, G. Feingold, and Z. Levin, 2006: Aerosol effects on the lifetime of shallow cumulus. *Geophys. Res. Lett.,* **33,** L14806, doi:10.1029/2006GL026024.

Kain, J. S., and J. M. Fritsch, 1993: Convective parameterization for mesoscale models: The Kain–Fritsch scheme. *The Representation of Cumulus Convection in Numerical Models, Meteor. Monogr.,* No. 46, Amer. Meteor. Soc., 165–170.

Klemp, J. B., and R. B. Wilhelmson, 1978: The simulation of three-dimensional convective storm dynamics. *J. Atmos. Sci.,* **35,** 1070–1096.

Laird, N. F., H. T. Ochs III, R. M. Rauber, and L. J. Miller, 2000: Initial precipitation formation in warm Florida cumulus. *J. Atmos. Sci.,* **57,** 3740–3751.

Lee, S. S., J. E. Penner, and S. M. Saleeby, 2009: Aerosol effects on liquid-water path of thin stratocumulus clouds. *J. Geophys. Res.,* **114,** D07204, doi:10.1029/2008JD010513.

Long, A., 1974: Solutions to the droplet collection equation for polynomial kernels. *J. Atmos. Sci.,* **31,** 1040–1052.

Lynn, B. H., A. P. Khain, J. Dudhia, D. Rosenfeld, A. Pokrovsky, and A. Seifert, 2005: Spectral (bin) microphysics coupled with a mesoscale model (MM5). Part I: Model description and first results. *Mon. Wea. Rev.,* **133,** 44–58.

Mather, G. K., 1991: Coalescence enhancement in large multicell storms caused by the emissions from a Kraft paper mill. *J. Appl. Meteor.,* **30,** 1134–1146.

Mellor, G. L., and T. Yamada, 1974: A hierarchy of turbulence closure models for planetary boundary layers. *J. Atmos. Sci.,* **31,** 1791–1806.

Meyers, M. P., R. L. Walko, J. Y. Harrington, and W. R. Cotton, 1997: New RAMS cloud microphysics parameterization. Part II. The two-moment scheme. *Atmos. Res.,* **45,** 3–39.

Pinsky, M., L. Magaritz, A. Khain, O. Krasnov, and A. Sterkin, 2008: Investigation of droplet size distributions and drizzle formation using a new trajectory ensemble model. Part I: Model description and first results in a nonmixing limit. *J. Atmos. Sci.,* **65,** 2064–2086.

Pruppacher, H., and J. Klett, 1997: *Microphysics of Clouds and Precipitation*. 2nd ed. Kluwer Academic, 954 pp.

Rosenfeld, D., 1999: TRMM observed first direct evidence of smoke from forest fires inhibiting rainfall. *Geophys. Res. Lett.,* **26,** 3105–3108.

Rudich, Y., O. Khersonsky, and D. Rosenfeld, 2002: Treating clouds with a grain of salt. *Geophys. Res. Lett.,* **29,** 2060, doi:10.1029/2002GL016055.

Saleeby, S. M., and W. R. Cotton, 2004: A large droplet mode and prognostic number concentration of cloud droplets in the Colorado State University Regional Atmospheric Modeling System (RAMS). Part I: Module descriptions and supercell test simulations. *J. Appl. Meteor.,* **43,** 182–195.

Smagorinsky, J., 1963: General circulation experiments with the primitive equations. I: The basic experiment. *Mon. Wea. Rev.,* **91,** 99–164.

Takemura, T., H. Okamoto, Y. Maruyama, A. Numaguti, A. Higurashi, and T. Nakajima, 2000: Global three-dimensional simulation of aerosol optical thickness distribution of various origins. *J. Geophys. Res.,* **105,** 17 853–17 873.

——, T. Nozawa, S. Emori, T. Y. Nakajima, and T. Nakajima, 2005: Simulation of climate response to aerosol direct and indirect effects with aerosol transport-radiation model. *J. Geophys. Res.,* **110,** D02202, doi:10.1029/2004JD005029.

Twomey, S., 1977: The influence of pollution on the shortwave albedo of clouds. *J. Atmos. Sci.,* **34,** 1149–1152.

Tzivion, S., G. Feingold, and Z. Levin, 1987: An efficient numerical solution to the stochastic collection equation. *J. Atmos. Sci.,* **44,** 3139–3149.

van den Heever, S. C., G. G. Carrió, W. R. Cotton, P. J. DeMott, and A. J. Prenni, 2006: Impacts of nucleating aerosol on Florida storms. Part I: Mesoscale simulations. *J. Atmos. Sci.,* **63,** 1752–1775.

Walko, R. L., W. R. Cotton, M. P. Meyers, and J. Y. Harrington, 1995: New RAMS cloud microphysics parameterization. Part I: The single-moment scheme. *Atmos. Res.,* **38,** 29–62.

——, and Coauthors, 2000: Coupled atmosphere–biophysics–hydrology models for environmental modeling. *J. Appl. Meteor.,* **39,** 931–944.

Wood, R., 2007: Cancellation of aerosol indirect effects in marine stratocumulus through cloud thinning. *J. Atmos. Sci.,* **64,** 2657–2669.

Xue, H., and G. Feingold, 2006: Large-eddy simulations of trade wind cumuli: Investigation of aerosol indirect effects. *J. Atmos. Sci.,* **63,** 1605–1622.